Soft Matter

PAPER

View Article Online
View Journal | View Issue

Cite this: *Soft Matter*, 2018, **14**, 7500

Nanoliter deposition on star-shaped hydrophilic–superhydrophobic patterned surfaces†

Bo Chang, *[ab] Oskari Kivinen,[b] Ivana Pini,[c] Pavel A. Levkin,[c] Robin H. A. Ras[bd] and Quan Zhou[e]

Received 24th June 2018,
Accepted 15th August 2018

DOI: 10.1039/c8sm01288a

rsc.li/soft-matter-journal

Nanoliter sized droplet deposition has gained increasing importance in many biomedical, chemical, and microfluidic applications and in materials synthesis. In this paper, we report a simple method for rapid and high-throughput deposition of nanoliter-sized droplets by dragging a larger droplet on star-shaped hydrophilic–superhydrophobic patterned surfaces. Dragging a droplet on the patterned surface causes water to adhere to hydrophilic patterns. As the larger mother droplet detaches from a star-shaped pattern, a small daughter droplet is deposited on the pattern. Star-shaped hydrophilic patterns with a distinct number of spikes are fabricated and investigated. Systematic tests are carried out to study the influence of different process parameters including the volume of a mother droplet, the dragging velocity, the number of spikes and the dragging directions to the deposition process. The results indicate that creating microarrays by dragging large droplets on patterned hydrophilic–superhydrophobic surfaces yield a reliable, cost-efficient, high-accuracy and easily scalable deposition. The volume of the daughter droplet grows with the velocity of the mother droplet and the number of spikes in a pattern, and decreases with the volume of the mother droplet.

1. Introduction

Nanoliter volume liquid deposition has gained increasing importance in many biomedical, chemical and microfluidic applications, such as droplet based microfluidic systems,[1] delivery of DNA,[2–4] cell screening,[5–8] protein chips[9,10] and material research.[11] Contact dispensing and non-contact dispensing are two classical techniques for droplet deposition. With increasing demand of high-accuracy and short cycle time, the non-contact dispensing method gains higher popularity. Top performance of a non-contact dispensing system can achieve throughput up to 96 samples in a few minutes and sub-nanoliter precision, with 4–8 tips pipetting simultaneously.[12–14] Other methods include dip-pen nanolithography technique and polymer pen lithography,[15,16] where nanoscale tips were used to write liquid patterns directly on a substance with different kinds of inks. Impressive results have been claimed, *e.g.* high-density microarrays were formed using 55 000 AFM tips in parallel with throughputs on the scale of 1 cm^2 per minute.[17] Despite the impressive results, these techniques also have their limitations. In contact dispensing, nanoliter liquid deposition is challenging; non-contact dispensing can reach nanoliter precision, the dispensing speed is largely compromised however; dip-pen nanolithography and polymer pen lithography can achieve high-throughput and high-accuracy deposition simultaneously by using a large amount of nanoscale tips in parallel, but the system is rather expensive. The pursuit of simple and cost-effective methods for the high-throughput and high-resolution nanoliter liquid deposition method is still ongoing. One potential solution is the utilization of hydrophilic–superhydrophobic patterned surfaces by either dipping it inside the water or moving the water droplets on patterned surfaces. Due to the strong dewetting effect of the water on the superhydrophobic surface, only the hydrophilic areas will be filled with water.[18–20] Numerous promising results have been claimed, for example, arrays of different shapes and different liquids such as aqueous solution, microparticles and hydrogels can be generated using patterned hydrophilic–superhydrophobic surfaces;[5–8] gravity-induced sliding droplets can achieve parallel nanoliter and multiple-liquid deposition using hydrophilic–superhydrophobic patterned surfaces.[21] Furthermore, hydrophilic–hydrophobic wettability patterns with different shapes, especially with star shapes, have attracted more interest due to their biomimetic features to the structures on the back of desert beetles and silk spiders for enhancing water collection.[22–27] However, most of the studies focused on the demonstration of droplet deposition using hydrophilic–superhydrophobic patterned surfaces. There is a lack

[a] *College of Mechanical and Electrical Engineering, Shaanxi University of Science and Technology, Xi'An 710021, P. R. China*
[b] *School of Science, Aalto University, FI-00076 Aalto, Finland. E-mail: bo.chang@aalto.fi*
[c] *Institute of Toxicology and Genetics, Karlsruhe Institute of Technology, 76344 Eggenstein-Leopoldshafen, Germany*
[d] *School of Chemical Engineering, Aalto University, FI-00076 Aalto, Finland*
[e] *School of Electrical Engineering, Aalto University, FI-00076 Aalto, Finland*

† Electronic supplementary information (ESI) available. See DOI: 10.1039/c8sm01288a

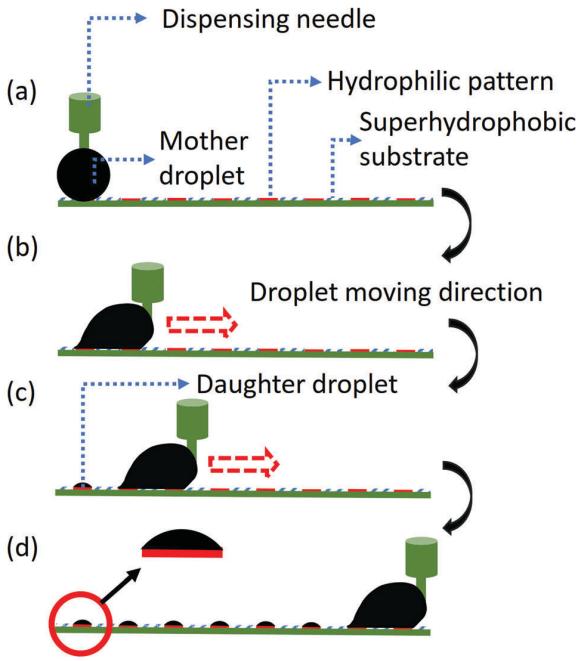

Fig. 1 Nanoliter droplet deposition using star-shaped hydrophilic–superhydrophobic patterned surfaces: (a) a mother droplet was dispensed on a star-shaped hydrophilic pattern using a dispensing needle; (b) the mother droplet was dragged by the needle and moved on to the patterned surface, and the edge of the mother droplet was pinned to the hydrophilic pattern; (c) as the mother droplet detached from the hydrophilic pattern, a small daughter droplet was deposited; (d) as the mother droplet reached the end of the patterned surface, all the star-shaped hydrophilic patterns were deposited with the same amount of water droplets.

of understanding about what are the parameters affecting the nanoliter water deposition process using star-shaped hydrophilic–superhydrophobic patterned surfaces.

In this paper, we design and fabricate star-shaped hydrophilic–superhydrophobic patterned surfaces to mimic the structures on the back of the desert beetles. We develop a deposition technique which can be used to efficiently deposit water on the patterned surfaces using a simple pipette-dragging technique. We employ a robotic system to study systematically the influence of process parameters including the dragging speed, the volume of the mother droplet, the number of spikes and dragging directions on water deposition. The proposed experimental investigation procedure is presented in Fig. 1. When a large mother droplet detaches from a hydrophilic pattern due to the relative motion between the needle and the sample surface, a daughter droplet is deposited on the pattern. A typical droplet deposition process is presented in the movie of the ESI.†

2. Experimental setup and test samples

2.1 Experimental setup

To study the nanoliter deposition process, a robotic system has been set up as shown in Fig. 2. The system consists of two microscopes, a dispensing system and a sample carrier. A dispensing needle was

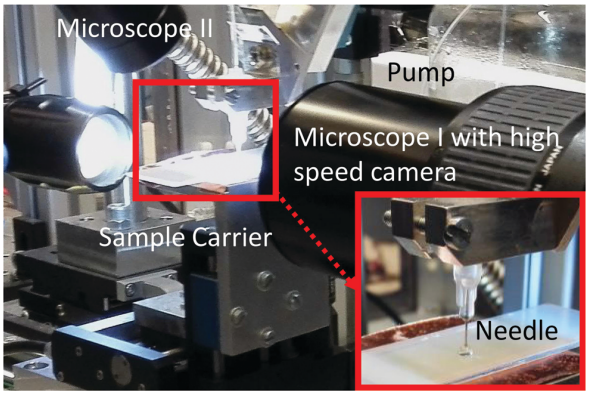

Fig. 2 Robotic system for carrying out nanoliter deposition on star-shaped hydrophilic–superhydrophobic patterned surfaces.

fixed to drag the water droplet on the sample and the patterned surface was placed onto a sample carrier. The sample carrier was built by combining three motorized stages (M-111.1DG, M-122.2DD and M-404.8PD by Physik Instrumente), which allowed movement in the *XYZ*-directions. The droplet motion was filmed from the side with a Phantom v1610 high-speed camera. The needle was manufactured by Drifton with an outer diameter of 0.41 mm and an inner diameter of 0.2 mm. The needle was attached to a Cavro Centris pump with a pipetting accuracy of 0.25% deviation at full stroke. The deposition process was also filmed with a Basler Scout scA1600 camera from a titled angle in order to investigate if all the star-shaped patterns were fully wetted.

2.2 Test samples

Star-shaped hydrophilic–superhydrophobic patterned surfaces with distinct number of spikes were designed and fabricated as shown in Fig. 3. The number of spikes varies from 3 to 10, and

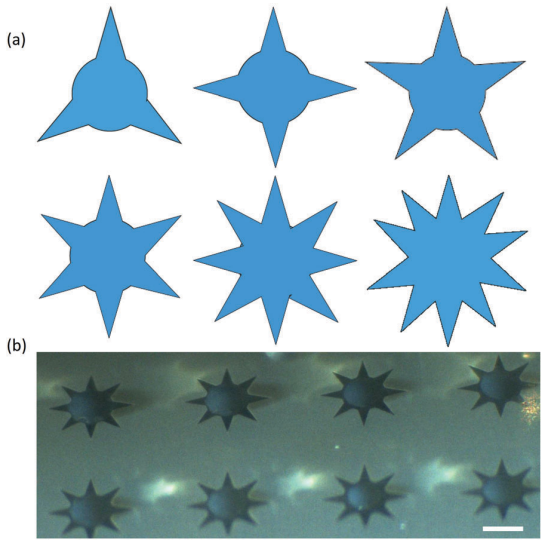

Fig. 3 (a) Design of star-shaped patterns; (b) star-shaped patterns with 8 spikes fully wetted by water droplets. Scale bar 500 μm.

the diameter of circular parts of the star-shaped patterns is 500 μm for all the samples. The length of all the spikes is 250 μm and the angle is 30°. The star-shaped patterns were fabricated on glass slides using a fabrication procedure adapted from previously published work.[8] Firstly, glass slides (Schott Nexterion, Jena, Germany) were immersed in 1 M sodium hydroxide solution (Merck KGaA, Darmstadt, Germany) for 1 h, then immersed in 1 M hydrochloric acid solution for 30 min. After that, 70 μL of 20% v/v ethanol and a 3-(trimethoxysilyl)propyl methacrylate solution (Sigma-Aldrich, Munich, Germany) were applied on the surface of the glass slides, followed by incubation for 30 min. Next, a 25 μL polymerization mixture containing 24 wt% 2-hydroxyethyl methacrylate (HEMA; Sigma-Aldrich), 16 wt% ethylene dimethacrylate (EDMA; Sigma-Aldrich), 12 wt% 1-decanol (Sigma-Aldrich, Munich, Germany), 48 wt% cyclohexanol (Sigma-Aldrich, Munich, Germany) and 0.4 wt% 2,2-dimethoxy-2-phenylacetophenone (DMPAP; Sigma-Aldrich) was applied on the glass slides and then covered by fluorinated glass slides, which were prepared by incubating glass slides overnight in a sealed desiccator containing an open vial with trichloro(1*H*,1*H*,2*H*,2*H*-perfluorooctyl)silane (Sigma-Aldrich) at 50 mbar. After that, the glass slides were polymerized *via* UV irradiation at 260 nm wavelength for 15 min with 10 mW cm^{-2} intensity using a deep-UV collimated light source (Model 30, Optical Associates Inc., San Jose, CA, USA) fitted with a 500 W Hg-xenon lamp (Ushio, Tokyo, Japan). The polymerized slides were then immersed in a mixture containing 45 mL of dichloromethane (Merck KGaA), 56 mg of 4-(dimethylamino)pyridine (DMAP; Novabiochem, Merck KGaA, Darmstadt, Germany), 111.6 mg of 4-pentanoic acid (Sigma-Aldrich) and 180 μL of *N*,*N*′-diisopropylcarbodiimide (DIC) solution (Alfa Aesar GmbH & Co. KG, Karlsruhe, Germany) under stirring for at least 4 h, and then washed with ethanol and dried using a nitrogen gun. The superhydrophobic substrate was created by applying 200 μL of 5% v/v perfluorodecanethiol solution (Sigma-Aldrich) in acetone onto the polymer surface, followed by UV-irradiation through a photomask (Rose Fotomasken, Bergisch Gladbach, Germany) at 260 nm wavelength for 1 min with 10 mW cm^{-2} intensity in the dark, followed by acetone washing and drying. The hydrophilic star-shaped patterns were created by applying 200 μL 10% v/v β-mercaptoethanol (Alfa Aesar) dissolved in 1 : 1 v/v water and ethanol solution onto the patterned surface, covering it with a quartz microscope slide (Science Services GmbH, Munich, Germany) and upon irradiation of the slide. The glass slides were finally washed with ethanol, dried using an air gun and ready for use. The thickness of the polymer is about 15 μm. Fig. 3b shows an array of fabricated star-shaped patterns with 8 spikes which are fully wetted by water droplets.

3. Results and discussion

A series of experiments have been carried out to study the influence of different process parameters including the dragging velocity, the volume of the mother droplet, the number of spikes and dragging directions on droplet deposition. Fig. 4a shows a

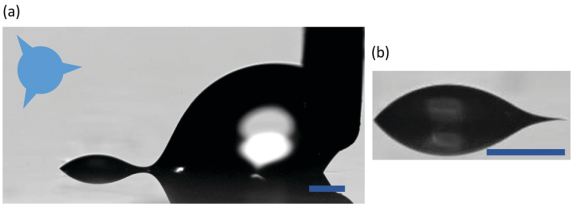

Fig. 4 (a) Droplet deposition on a 3-spike hydrophilic–superhydrophobic patterned surface; (b) image of a deposited daughter droplet on a 3-spike pattern. Scale bars 250 μm.

2-microliter mother droplet moving at a speed of 10 mm s^{-1} on a 3-spike patterned surface where a daughter droplet is formed. To estimate the deposition volume, we can treat a deposited daughter droplet as a spherical cap. To find out the influences of different parameters on deposition results, high-speed videos were filmed to detect the volume of the daughter droplet adhering to the hydrophilic patterns. The videos contained the travel of the mother droplet in a straight line over 7 star-shaped patterns with the same number of spikes. The test was repeated 4 times to minimize random errors. In total, 28 tests were carried out for the pattern with the same shape. The volume of each deposited daughter droplet was calculated using a Matlab™ script based on the parameters determined from the image shown in Fig. 4b.

3.1 Influence of dragging velocity

The mother droplet was dragged over star-shaped patterns of 3 spikes at velocities of 5, 10, 15 and 20 mm s^{-1}. Fig. 5 shows the relationship between the volume of the daughter droplet and the dragging velocity. The dots represent the mean deposited volumes and are linked using dashed lines. The error bars represent the standard derivations of the deposited volume of the daughter droplet based on the 28 independent measurements for each dragging velocity. For each dragging velocity, three volumes of 1, 2, and 3 microliters of the mother droplet were tested. The results show that the volume of the deposited daughter droplet increases with the dragging velocity independent of the volume of the mother droplet.

We attribute this to the oscillation of the mother droplet. The oscillation of the mother droplet comes from the repeated pinning, depinning and rupture events, including the pinning

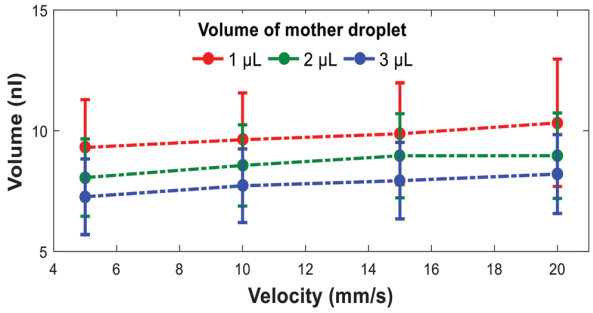

Fig. 5 Influence of the dragging velocity on the volume of the daughter droplet. The volume increases as the dragging velocity increases.

of the front edge of the mother droplet on the patterns, the depinning of the mother droplet from the superhydrophobic substrate and the rupture between the mother droplet and the daughter droplet. Since the spacing of the star-shaped patterns is the same, the higher is the velocity, the higher is the frequency of those pinning, depinning, rupture events, which leads to a great level of oscillation of the mother droplet. The greater oscillation of the mother droplet increases the energy of the mother droplet. The higher the energy of a mother droplet has, the easier can the daughter droplet detach from it. Consequently, a high velocity of the mother droplet leads to a greater mean volume of the daughter droplet. On the other hand, the oscillation of the mother droplet can also lead to a great variation in deposition, especially when the volume of the mother droplet is relatively small.

3.2 Influence of volume of the mother droplet

To study the influence of the volume of the mother droplet on deposition, 28 tests were carried out for the mother droplet of volume 1, 2, and 3 microliters respectively using patterns with 3 spikes. Fig. 6 shows the relationship between the volume of the mother droplet and the volume of the deposited daughter droplet, where the dots represent the mean volume of the daughter droplet and the error bars represent the standard derivations of the deposited daughter droplet. The dragging velocity was kept the same as 5 mm s^{-1}, 10 mm s^{-1}, 15 mm s^{-1} and 20 mm s^{-1} respectively for each test.

The results show that the volume of the daughter droplet decreases slightly as the volume of the mother droplet increases from 1 microliter to 3 microliters, largely independent of the dragging velocity. This correlation can be explained based on the assumption that the Laplace pressure of a mother droplet equals to the Laplace pressure of a daughter droplet at the moment of splitting up. Since the velocity of the mother droplet is much smaller than the speed of surface-tension induced phenomena (*e.g.* wetting or forming droplet), the system can be treated as quasi-static. Therefore, the pressure inside the spherical cap-shaped mother droplet/daughter droplet before rupture can be treated as constant. The Laplace pressure of a mother droplet and a daughter droplet can be written as

$$\Delta P_{\text{mother}} = \frac{2\gamma}{R} = \Delta P_{\text{daughter}} = \frac{2\gamma}{r}. \quad (1)$$

where R and r are the principal radii of the mother droplet and the daughter droplet correspondingly. Therefore, the principal radius of the mother droplet and the daughter droplet should be the same:

$$R = r \quad (2)$$

The volume of the resulted daughter droplet can be calculated as a spherical cap:

$$V_{\text{d}} = \frac{\pi h_{\text{d}}}{6}\left(3a^2 + h_{\text{d}}^2\right). \quad (3)$$

where h_{d} is the height of the daughter droplet, and a is the base radius of the daughter droplet as shown in Fig. 7.

The height of the daughter droplet can be described as

$$h_{\text{d}} = r - \sqrt{r^2 - a^2} \quad (4)$$

For a given pattern, the base radius of the daughter droplet a is fixed, so the volume V_{d} is proportional to h_{d}^3, and h_{d} is inversely proportional to r. Therefore, the volume of the daughter droplet V_{d} decreases with greater r. The volume of the mother droplet can also be calculated as a spherical cap:

$$V_{\text{m}} = \frac{\pi h_{\text{m}}}{6}\left(3a^2 + h_{\text{m}}^2\right). \quad (5)$$

where h_{m} is the height of the mother droplet, which can be calculated as:

$$h_{\text{m}} = R + \sqrt{R^2 - a^2}. \quad (6)$$

Fig. 8 shows the simulation results of the relation between both the volume of the daughter droplet and the mother droplet as a function of the principal radius of daughter droplet. In this simulation, the radius of the daughter droplet r varies from 400 to 600 μm and the base radius a is 250 μm. The volumes of the daughter droplet and the mother droplet were calculated based on eqn (3) and (5) correspondingly. The results indicate that when the volume of the mother droplet increases, the radius of the daughter droplet increases and the

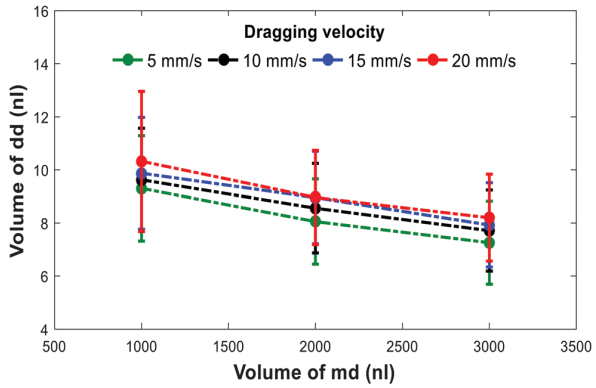

Fig. 6 Influence of the volume of the mother droplet on the volume of the daughter droplet. The volume of the daughter droplet decreases as the volume of the mother droplet increases.

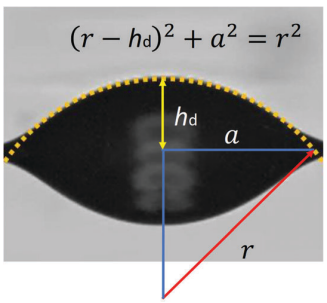

Fig. 7 A spherical cap-shaped daughter droplet with radius r, height h_{d} and base radius a.

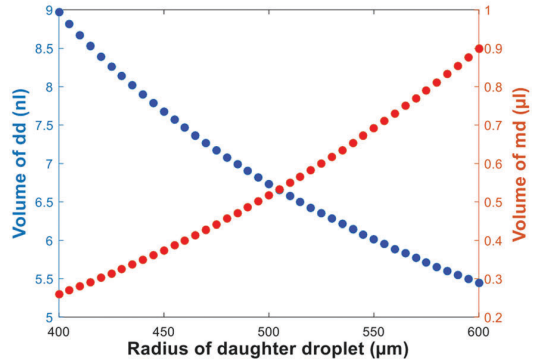

Fig. 8 Simulation of the volume of the daughter droplet and the mother droplet as a function of the radius of the daughter droplet.

volume of the daughter droplet decreases. This is the reason that a larger mother droplet tends to produce a smaller daughter droplet.

3.3 Influence of the number of spikes

We tested patterns with a number of spikes of 3, 4, 5, 6, 8 and 10. The dragging velocity was kept the same as 5 mm s^{-1}, 10 mm s^{-1}, 15 mm s^{-1} and 20 mm s^{-1} respectively for each test. Fig. 9 shows the relation between the number of spikes of the hydrophilic patterns and the volume of the deposited daughter droplet as well as the geometrical area of the corresponding patterns. The left vertical axis represents the volume of the deposited daughter droplet, and the right vertical axis represents the area of the hydrophilic patterns. The images of star-shaped patterns demonstrate that they are fully wetted by water droplets. The solid blue squares represent the area of the patterns with the corresponding number of spikes. The number of spikes has a positive correlation with the volume of a daughter droplet and the wetted area independent of the dragging velocity. The increase in volume can be attributed to the increased total wetted area of the pattern when the number of spikes increases. Furthermore, the number of the spikes affects the shape of the meniscus which could also influence the deposition volume.

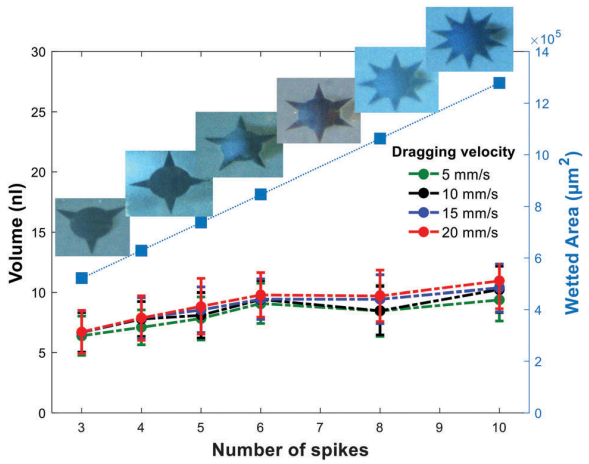

Fig. 9 Influence of the number of spikes on the volume of the daughter droplet. The deposition volume and wetted area increase as the number of spikes increases.

3.4 Influence of dragging directions

Besides the volume of the mother droplet and the dragging speed, the influence of dragging directions was also investigated. Patterns with 3 spikes were tested. Fig. 10 shows dragging directions (transverse, longitudinal positive and longitudinal negative) and their influence on the deposition results. The transverse direction yields a smaller volume of deposition compared to the longitudinal directions, and the positive longitudinal direction yields a slightly larger volume compared to the negative direction. When a droplet is dragged in the transverse direction, there is no spike pointing to the moving direction, whereas longitudinal directions have one spike pointing out towards the axis. Moreover, the slight difference between the positive and negative longitudinal directions originates from the patterns where the positive direction has a spike pointing out to the moving direction and the negative direction does not. The results indicate that a shape with a spike pointing out to the moving direction increases the volume of the daughter droplet.

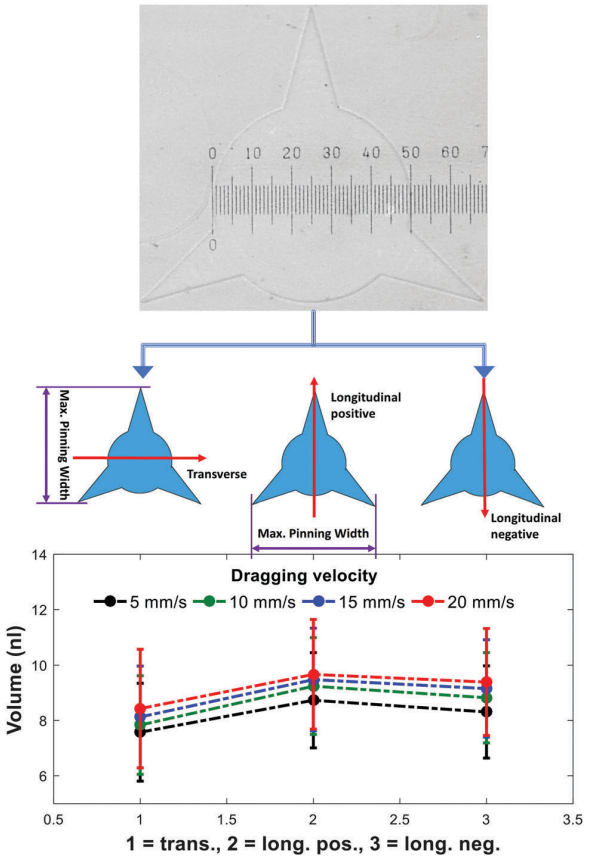

Fig. 10 Influence of the dragging direction on the volume of the daughter droplet. Transverse (trans.) direction appears to result in a smaller volume of the daughter droplet. The difference in longitudinal directions is relatively small.

This might be reasoned by studying the detachment process of a mother droplet. The pinning force can be calculated by

$$F = L\gamma(\cos\theta_r - \cos\theta_a). \quad (7)$$

where L is the pinning width of the mother droplet, γ is the interfacial tension between water and gas, θ_r and θ_a are the receding and advancing contact angles of the droplet on the surface correspondingly. The difference in the deposition volume between the transverse and the longitudinal directions comes from the difference in the maximum pinning width. The pinning width is the projection of the pinning line on the axis orthogonal to the motion of the mother droplet. We measured the maximum pinning width based on the geometrical properties illustrated in Fig. 10 using an optical image of the 3-spike pattern with a micro-ruler (0.01 mm increments). The pinning force is proportional to the water–gas interfacial tension, the pinning width of the droplet and the contact angle hysteresis, as described in eqn (7).[28] When a mother droplet is moving along the longitudinal direction, the measured maximum pinning width is 856 μm which is greater than the transverse case of 738 μm. Given that both water–gas interfacial tension and contact angle hysteresis are constant, the corresponding maximum pinning force in the case of the longitudinal direction should be greater than the case of the transverse direction. Moreover, the total energy increase on the droplet should be equal to the work of the pinning force on the droplet. Given that the volume of the mother droplet is much greater than the daughter droplet, we can assume that the displacement of the mother droplet is similar to different pinning forces. Hence, a greater pinning force leads to greater work, which leads to a greater increase of the total energy of the mother droplet. We attribute the greater daughter droplet volume to this greater increase of energy. The minor difference between the longitudinal positive and longitudinal negative cases is also observed.

4. Conclusions

This paper describes the influence of the volume of a mother droplet, the dragging speed, the number of spikes and dragging directions on the volume of deposition on star-shaped hydrophilic–superhydrophobic patterned surfaces. The results show that the volume of the daughter droplet grows with the velocity of the mother droplet and the number of spikes in a pattern and decreases with the volume of the mother droplet. Furthermore, the dragging directions could also affect the volume of the deposition. The accuracy of the droplet deposition is mainly dependent on the precision of the fabricated hydrophilic patterns. The robotic system ensures high experimental repeatability. This deposition method should be applicable to other water-based solvents even suitable for oil-based solution if oleophilic–superoleophobic patterned surfaces are used. The proposed method can be easily scaled-up by employing a row of liquid dispensers, enabling this method to be applicable in a potential larger scale and high-throughput production of arrays of nanoliter-sized droplets.

Conflicts of interest

There are no conflicts to declare.

Acknowledgements

This research was supported by the Academy of Finland's Centres of Excellence Programme (HYBER, 2014-2019), the National Natural Science Foundation of China (Grant no. 61703255), the European Research Council (ERC) under the European Union's Horizon 2020 research and innovation programme (Grant agreement No. 725513) and the ERC Starting Grant (337077-DropCellArray).

References

1 G. M. Whitesides, *Nature*, 2006, **442**, 368–373.
2 K.-H. Kim, R. G. Sanedrin, A. M. Ho, S. W. Lee, N. Moldovan, C. A. Mirkin and H. D. Espinosa, *Adv. Mater.*, 2008, **20**, 330.
3 T. Friedrich, S. Rahmann, W. Weigel, W. Rabsch, A. Fruth, E. Ron, F. Gunzer, T. Dandekar, J. Hacker, T. Muller and U. Dobrindt, *BMC Genomics*, 2010, **11**, 591.
4 G. C. Le Goff, J. C. Brès, D. Rigal, L. J. Blum and C. A. Marquette, *Anal. Chem.*, 2010, **82**, 6185–6192.
5 E. Ueda, F. L. Geyer, V. Nedashkivska and P. A. Levkin, *Lab Chip*, 2012, **12**, 5218.
6 W. Feng, L. Li, E. Ueda, J. Li, S. Heißler, A. Welle, O. Trapp and P. A. Levkin, *Adv. Mater. Interfaces*, 2014, **1**, 1400269.
7 J. J. Agresti, E. Antipov, A. R. Abate, K. Ahn, A. C. Rowat, J.-C. Baret, M. Marquez, A. M. Klibanov, A. D. Griffiths and D. A. Weitz, *Proc. Natl. Acad. Sci. U. S. A.*, 2010, **107**, 4004–4009.
8 G. Jogia, T. Tronser, A. Popova and P. Levkin, *Microarrays*, 2016, **5**, 28.
9 P. O. B. Mark Schena, D. Shalon and R. W. Davis, *Science*, 1995, **270**, 467–470.
10 R. S. Gaster, D. A. Hall and S. X. Wang, *Nano Lett.*, 2011, **11**, 2579–2583.
11 H. Jung, C. Ve Cheah, N. Jeong and J. Lee, *Appl. Phys. Lett.*, 2014, **105**, 053902.
12 J. Nakane, D. Broemeling, R. Donaldson, A. Marziali, T. D. Willis, M. O'Keefe and R. W. Davis, *Genome Res.*, 2001, **11**, 441–447.
13 M. Herklotz, M. Melamed, C. Trautmann, M. Nitschke, T. Pompe, F. U. Gast, F. Howitz and C. Werner, *Microfluid. Nanofluid.*, 2007, **3**, 629–633.
14 S. Melamed, L. Ceriotti, W. Weigel, F. Rossi, P. Colpo and S. Belkin, *Lab Chip*, 2011, **11**, 139–146.
15 R. D. Piner, *Science*, 1999, **283**, 661–663.
16 K. Salaita, Y. Wang and C. a. Mirkin, *Nat. Nanotechnol.*, 2007, **2**, 145–155.
17 O. A. Nafday and S. Lenhert, *Nanotechnology*, 2011, **22**, 225301.
18 A. A. Darhuber, S. M. Troian, J. M. Davis, S. M. Miller and S. Wagner, *J. Appl. Phys.*, 2000, **88**, 5119.
19 J. Huang, R. Fan, S. Connor and P. Yang, *Angew. Chem., Int. Ed.*, 2007, **46**, 2414–2417.

20 R. J. Jackman, D. C. Duffy, E. Ostuni, N. D. Willmore and G. M. Whitesides, *Anal. Chem.*, 1998, **70**, 2280–2287.
21 B. Chang, Q. Zhou, R. H. A. Ras, A. Shah, Z. Wu and K. Hjort, *Appl. Phys. Lett.*, 2016, **108**, 154102.
22 H. Bai, L. Wang, J. Ju, R. Sun, Y. Zheng and L. Jiang, *Adv. Mater.*, 2014, **26**, 5025–5030.
23 S. C. Thickett, C. Neto and A. T. Harris, *Adv. Mater.*, 2011, **23**, 3718–3722.
24 Y. Chen, D. Li, T. Wang and Y. Zheng, *Sci. Rep.*, 2016, **6**, 1–7.
25 L. Zhai, M. C. Berg, F. Ç. Cebeci, Y. Kim, J. M. Milwid, M. F. Rubner and R. E. Cohen, *Nano Lett.*, 2006, **6**, 1213–1217.
26 L. Zhang, J. Wu, M. N. Hedhili, X. Yang and P. Wang, *J. Mater. Chem. A*, 2015, **3**, 2844–2852.
27 Z. Yu, F. F. Yun, Y. Wang, L. Yao, S. Dou, K. Liu, L. Jiang and X. Wang, *Small*, 2017, **13**, 1–6.
28 S. J. Hong, C. C. Chang, T. H. Chou, Y. J. Sheng and H. K. Tsao, *J. Phys. Chem. C*, 2012, **116**, 26487–26495.